Supplementary Figures to

Bioavailable atmospheric phosphorous supply to the global ocean: a 3-D global modelling study

by *S. Myriokefalitakis et al.*

Figure S1. Annual averaged distributions of TP emissions (in ng-P m^{-2} s^{-1}) originated from a) mineral dust, b) anthropogenic combustion (sum of fossil fuel and biofuel combustion), c) biomass burning, d) PBAP, e) sea-spray and f) volcanic eruptions, taking into account by the TM4-ECPL model for the present atmosphere.

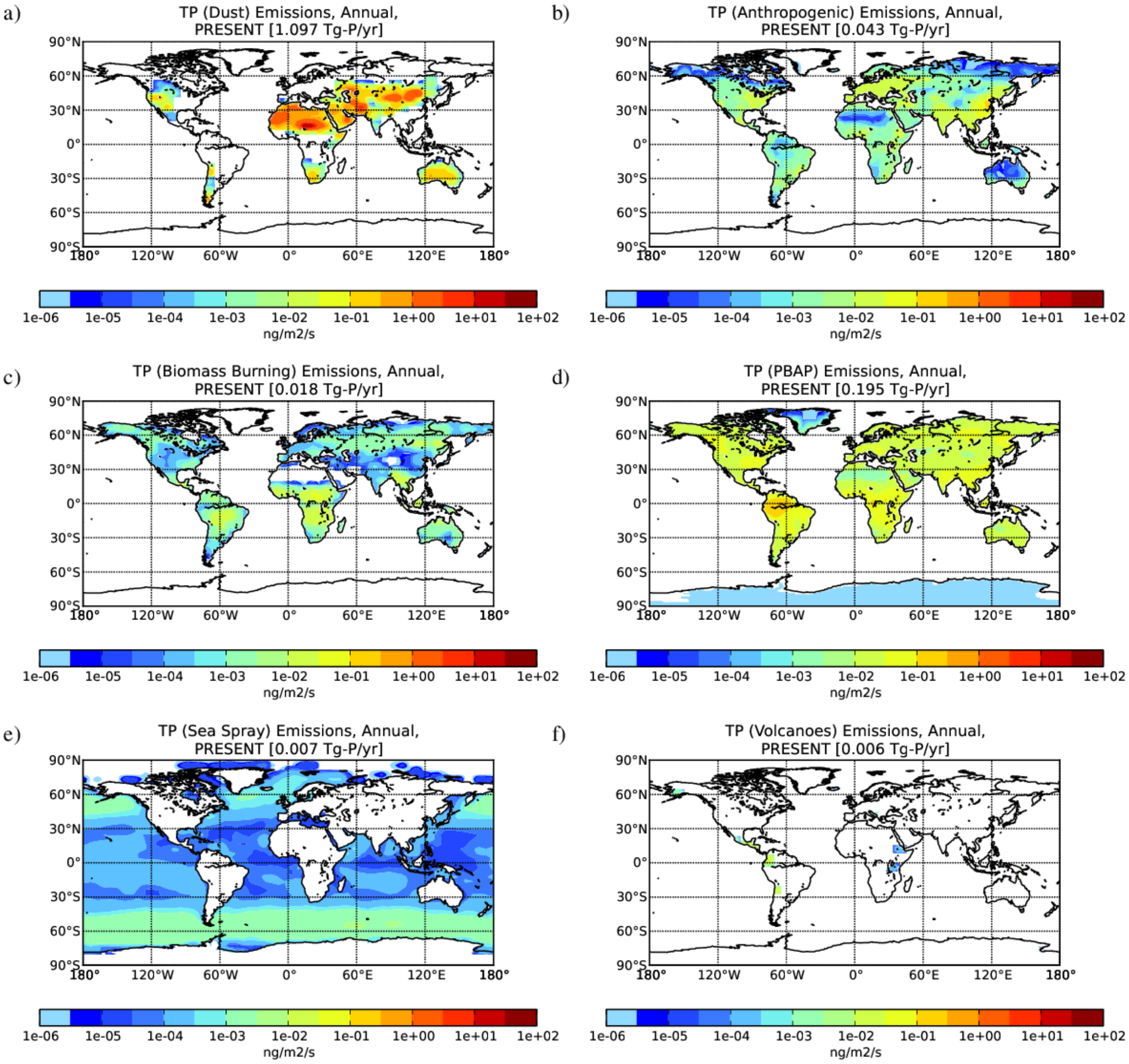

Figure S2. Annual averaged distributions of DP emissions (in ng-P m^{-2} s^{-1}) originated a) mineral dust, b) anthropogenic combustion (sum of fossil fuel and biofuel combustion), c) biomass burning, d) PBAP, e) sea-spray and f) volcanic eruptions, taking into account by the TM4-ECPL model for the present atmosphere.

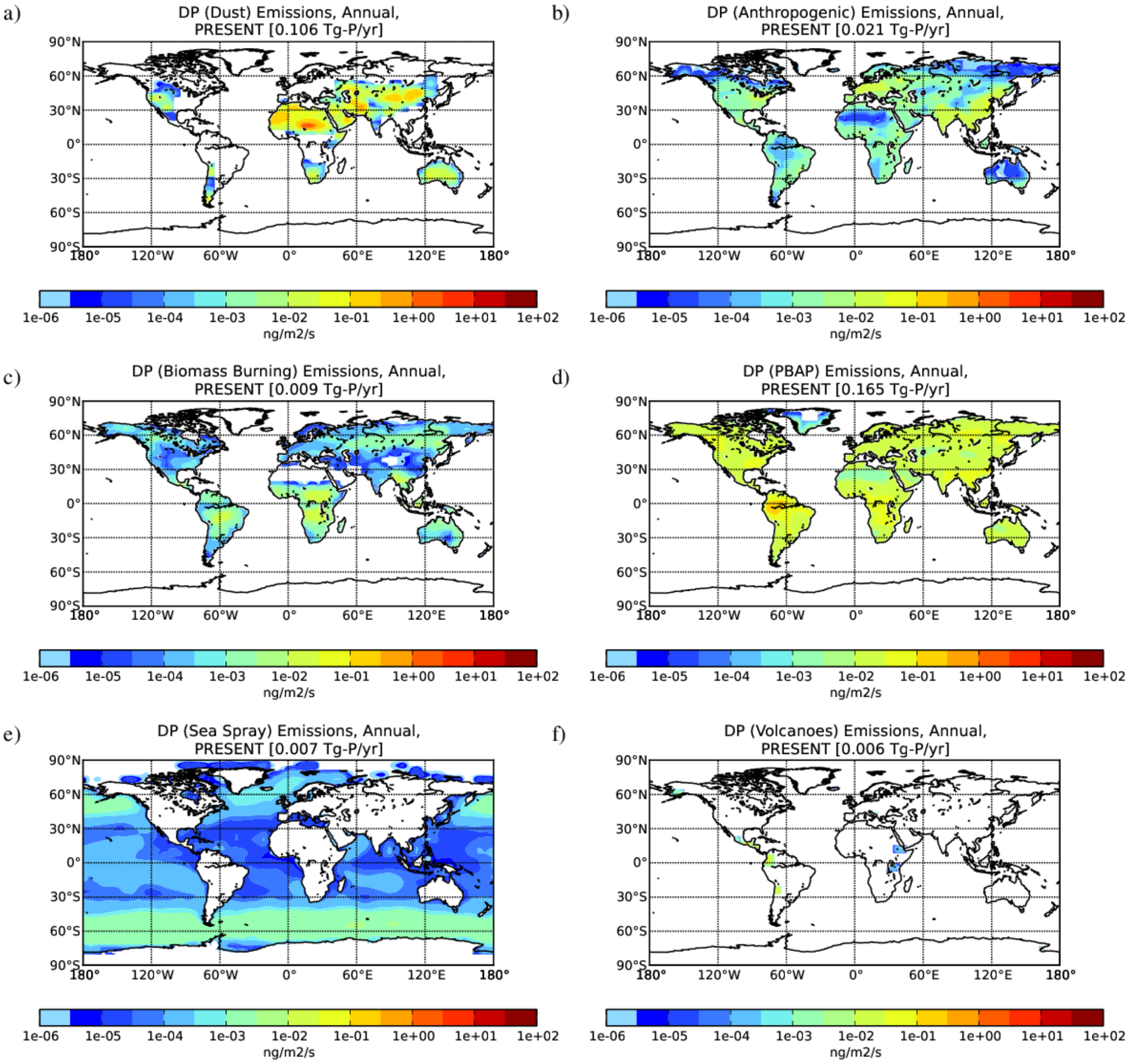

a) DP (Dust) Emissions, Annual, PRESENT [0.106 Tg-P/yr]

b) DP (Anthropogenic) Emissions, Annual, PRESENT [0.021 Tg-P/yr]

c) DP (Biomass Burning) Emissions, Annual, PRESENT [0.009 Tg-P/yr]

d) DP (PBAP) Emissions, Annual, PRESENT [0.165 Tg-P/yr]

e) DP (Sea Spray) Emissions, Annual, PRESENT [0.007 Tg-P/yr]

f) DP (Volcanoes) Emissions, Annual, PRESENT [0.006 Tg-P/yr]

Figure S3. Calculated annual fluxes (in ng-P m^{-2} s^{-1}) of FAP (left column; a,c,e) dissolution and HAP dissolution (right column; b,d,f) in aerosol water (upper figures; a,b), only in (middle figures; c,d) and only in cloud droplets (bottom figures; e,f), as calculated by the TM4-ECPL model for the present atmosphere.

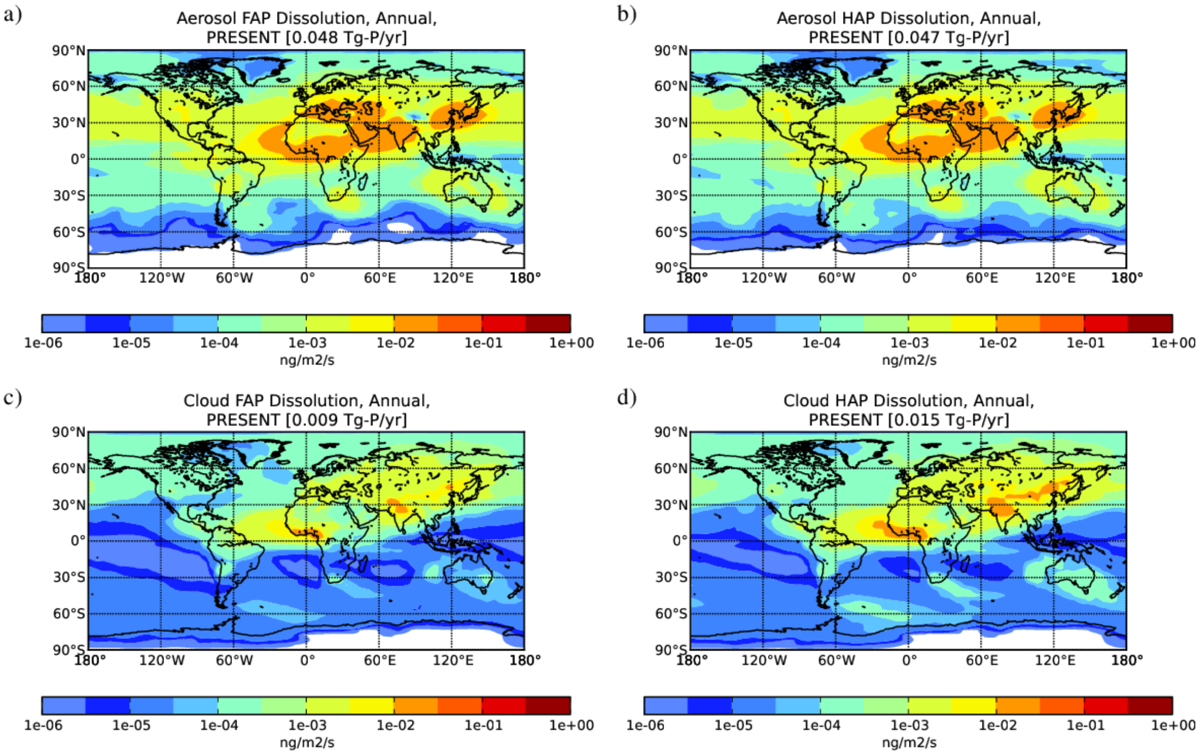

Figure S4. Log-scatter plot of model (y-axis) comparison against observations (x-axis) for a) TP surface concentrations, b) PO4 surface concentrations, c) PO4 dry deposition fluxes and d) PO4 wet deposition fluxes, with red circles for PRESENT simulation (Base), green stars for taking into account Wang et al. (2014) anthropogenic and natural combustion P emissions (W14-Comb.Emis) and blue crosses for neglected PO4 mobilization due to apatite dissolution (No-Dissolution). The continuous black line shows the 1:1 correlation and the dashed black lines show the 10:1 and 1:10 relationships, respectively. Atmospheric concentrations are observed by Baker et al. (2010), Martino et al. (2014) and Powell et al. (2015) and from unpublished measurements (Mihalopoulos and co-workers) as observed in the Finokalia Station (35°20′ N, 25°40′ E, Greece) and in the Corsica Island (42°40′ N, 9°04′ E, France). Deposition fluxes are taken from Vet et al. (2014) compilation and from unpublished measurements (Mihalopoulos and co-workers) as observed in the Finokalia Station.

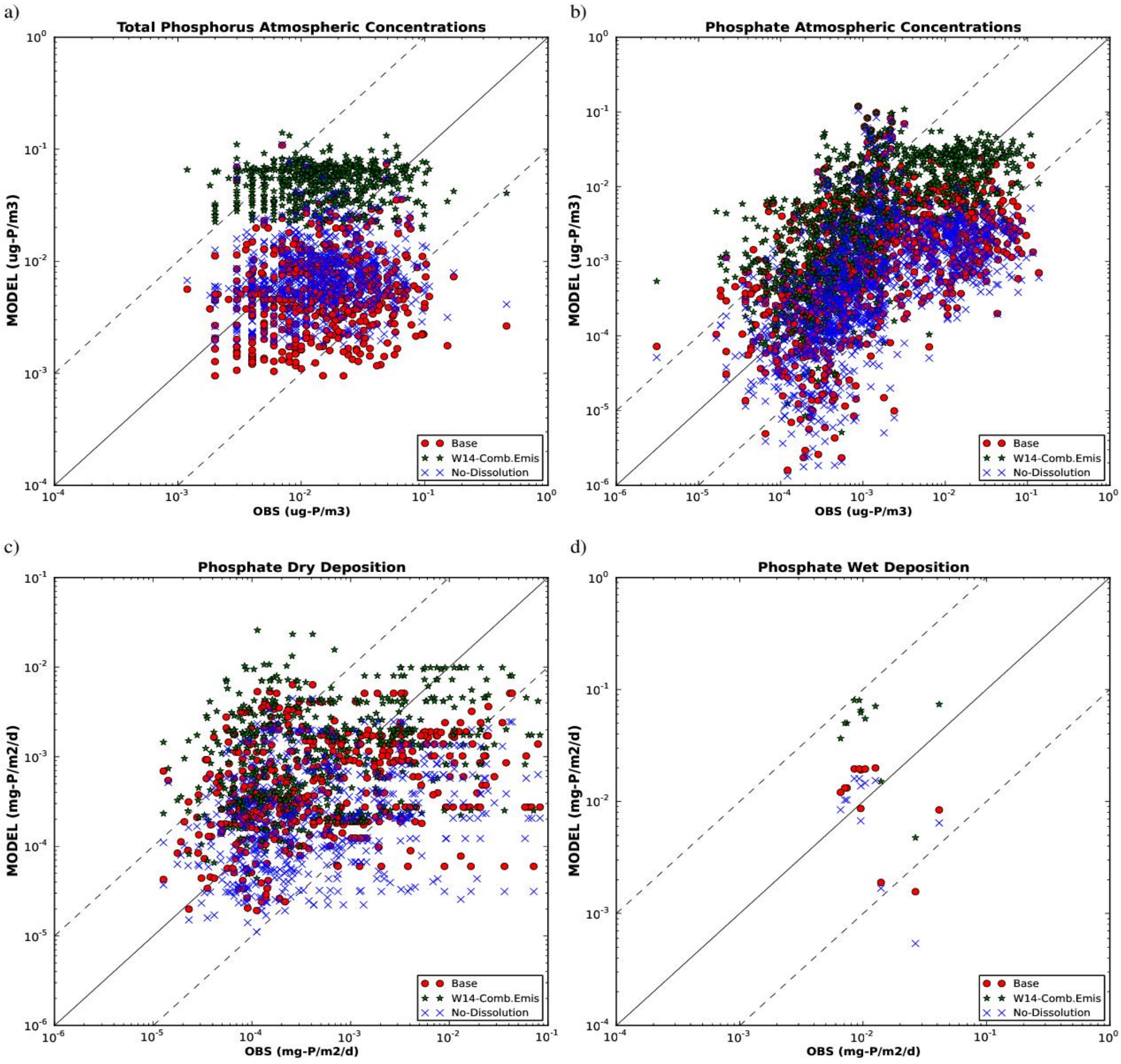

Figure S5. Annual variation of PO4 and TP concentrations (in µg-P m^{-3}) as observed by Baker et al. (2010), Martino et al. (2014) and Powell et al. (2015) in cruises over the Atlantic Ocean and by Mihalopoulos and co-workers (unpublished data) at the Finokalia Station (35°20′ N, 25°40′ E, Greece) in Eastern Mediterranean and the in Corsica Island (42°40′ N, 9°04′ E, France). All observations (black crosses and dots) are averaged per day (or month) taking into account the standard deviation (grey vertical lines) and validated against the respective TM4-ECPL model results (red line for PRESENT simulation, green line for taking into account Wang et al. (2014) anthropogenic and natural combustion P emissions and blue dashed lines with neglected PO4 mobilization due to apatite dissolution).

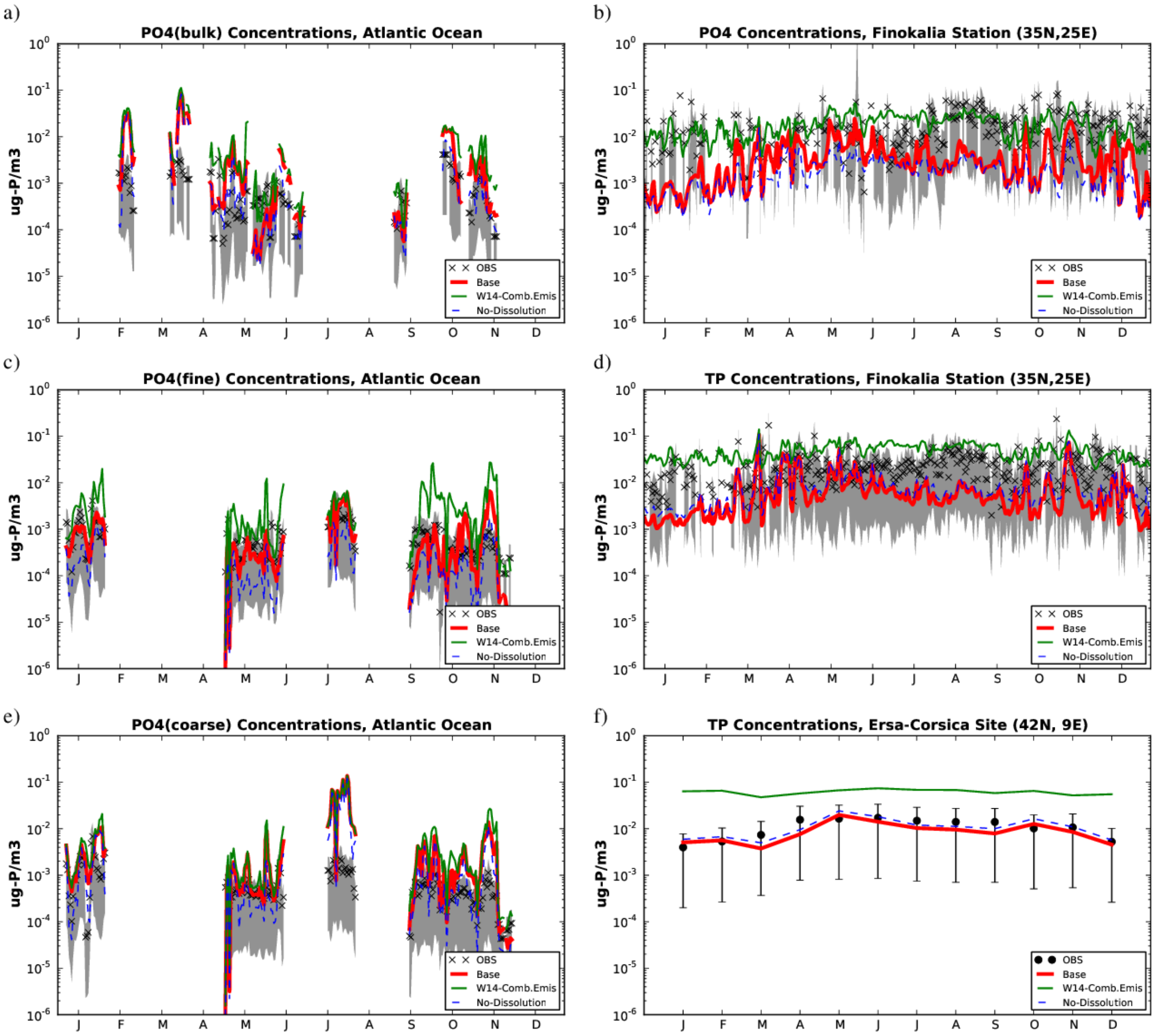

Figure S6. Annual variation of PO4 and TP deposition fluxes (in mg-P m^{-2} day^{-1}) as compiled by Vet et al. (2014) and as measured from Mihalopoulos and co-workers in Finokalia Station (35°20′ N, 25°40′ E, Greece) in the Eastern Mediterranenan. All observations (black dots) are averaged per month taking into account the standard deviation (grey vertical lines) and validated against TM4-ECPL monthly model results (red line for PRESENT simulation, green line for taking into account Wang et al. (2014) anthropogenic and natural combustion P emissions and blue dashed lines with neglected PO4 mobilization due to apatite dissolution).

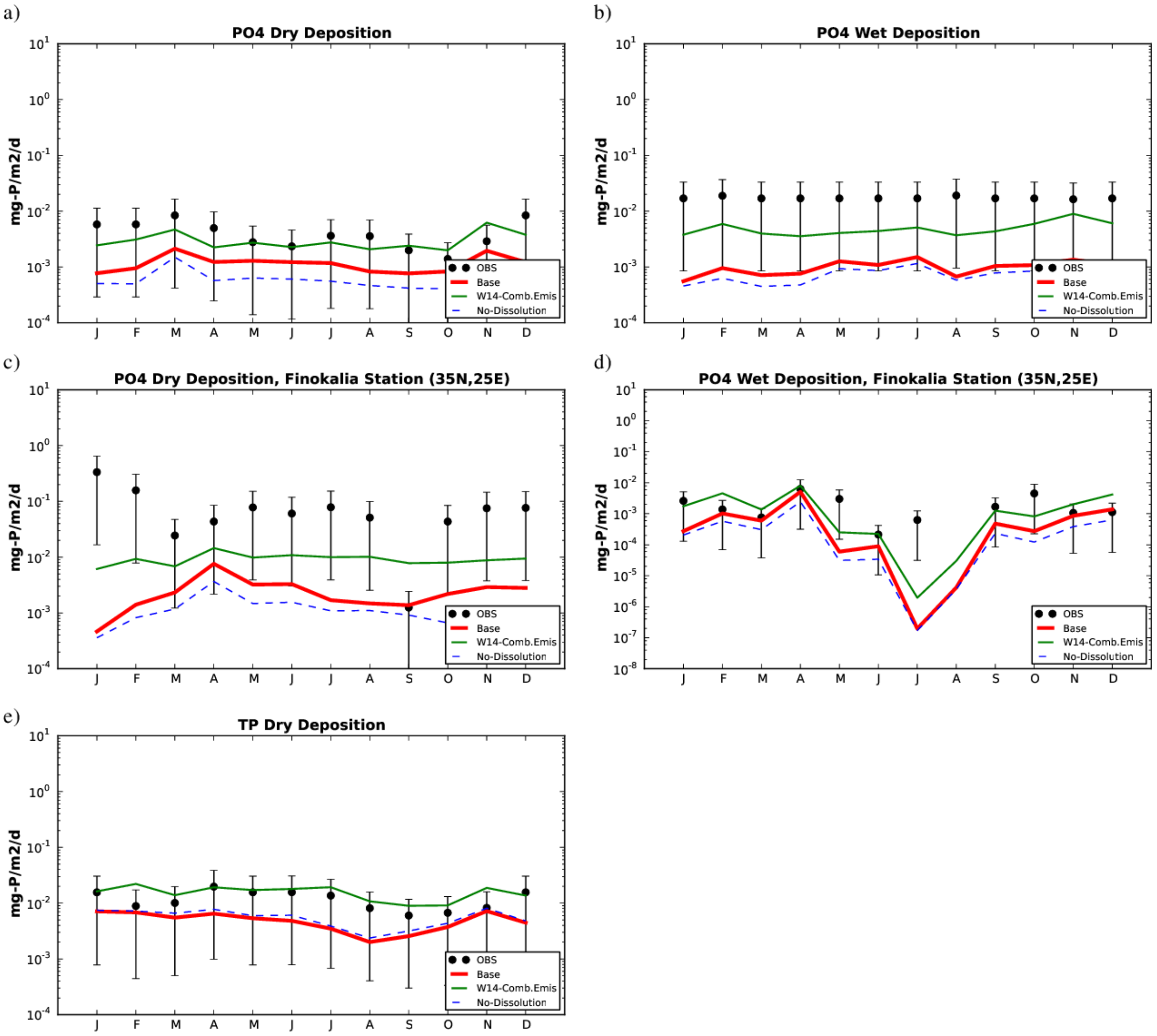

Figure S7. Calculated seasonal DP deposition fluxes (in ng-P m^{-2} s^{-1}) for a) December, January and February (DJF); b) March, April and May (MAM); c) June, July and August (JJA) and d) September, October and November (SON). Within brackets the amounts of DP deposition over the globe (in parentheses only over ocean) are also provided.

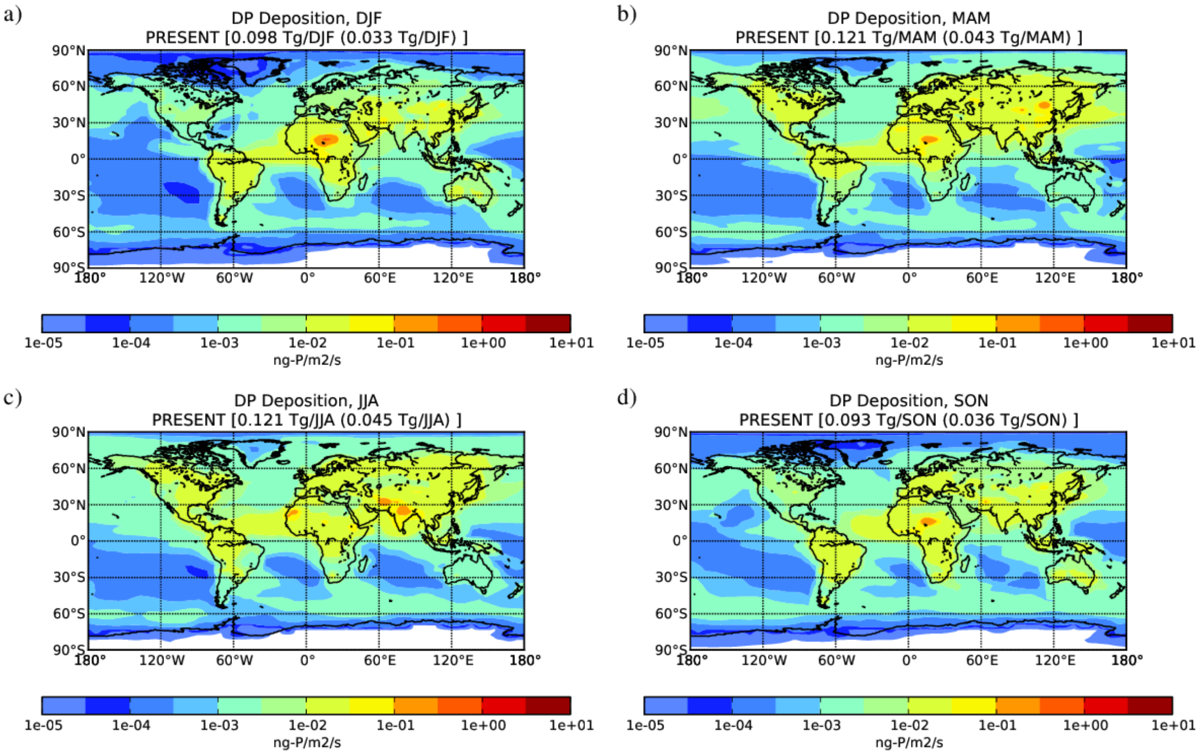

Figure S8. Calculated seasonal DP deposition fluxes (in ng-P m^{-2} s^{-1}) for dust (a-d) and PBAP (e-h) for a,e) December, January and February (DJF); b,f) March, April and May (MAM); c,g) June, July and August (JJA) and d,h) September, October and November (SON). Within brackets the amounts of DP deposition over the globe (in parentheses only over ocean) are also provided.

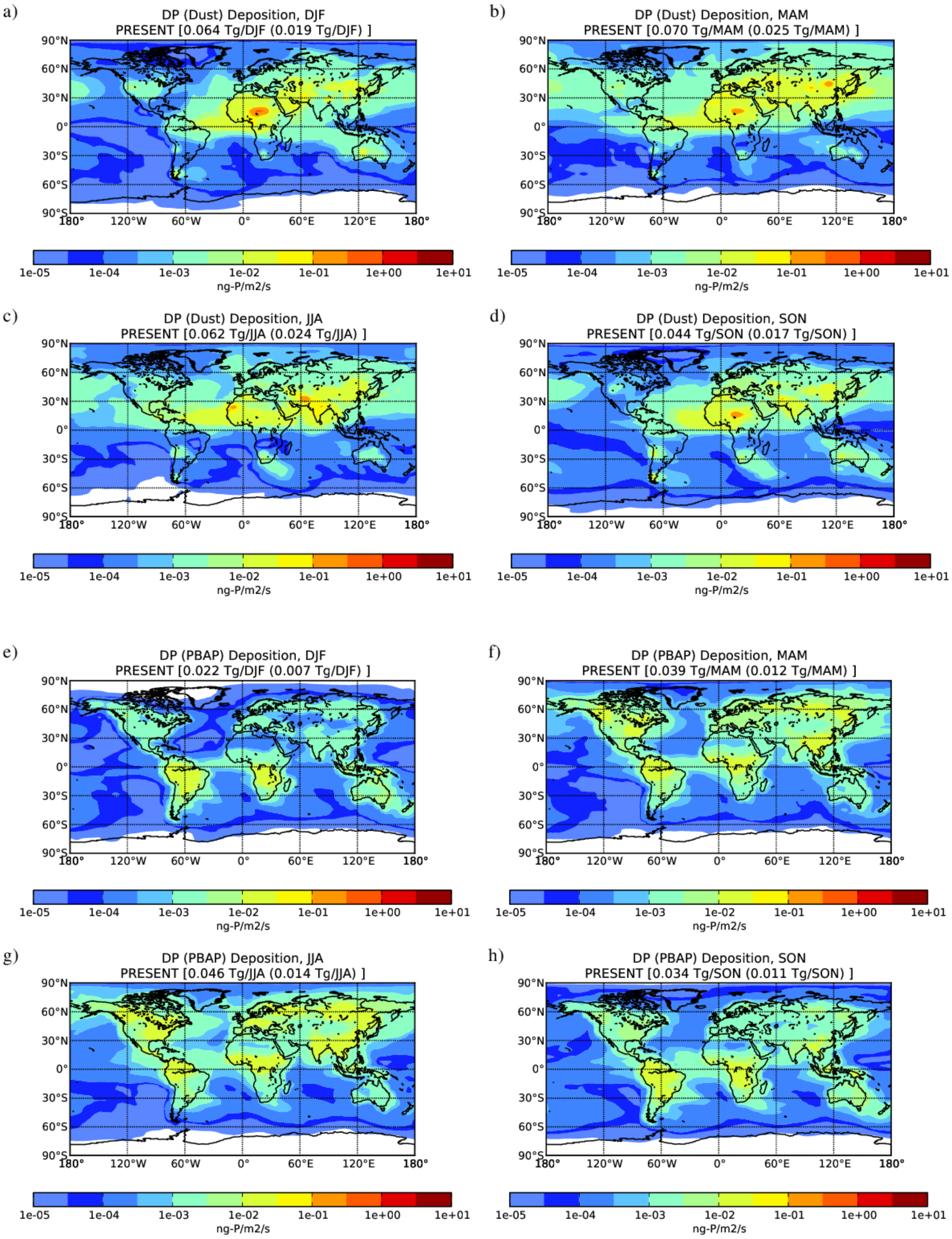

a) DP (Dust) Deposition, DJF
PRESENT [0.064 Tg/DJF (0.019 Tg/DJF)]

b) DP (Dust) Deposition, MAM
PRESENT [0.070 Tg/MAM (0.025 Tg/MAM)]

c) DP (Dust) Deposition, JJA
PRESENT [0.062 Tg/JJA (0.024 Tg/JJA)]

d) DP (Dust) Deposition, SON
PRESENT [0.044 Tg/SON (0.017 Tg/SON)]

e) DP (PBAP) Deposition, DJF
PRESENT [0.022 Tg/DJF (0.007 Tg/DJF)]

f) DP (PBAP) Deposition, MAM
PRESENT [0.039 Tg/MAM (0.012 Tg/MAM)]

g) DP (PBAP) Deposition, JJA
PRESENT [0.046 Tg/JJA (0.014 Tg/JJA)]

h) DP (PBAP) Deposition, SON
PRESENT [0.034 Tg/SON (0.011 Tg/SON)]

Figure S9. Annual mean percentage solubility in deposited P-containing aerosols (SP = %DP/TP) due a) mineral dust, b) anthropogenic combustion (sum of fossil fuel and biofuel combustion), c) biomass burning, d) PBAP, e) sea-spray and f) volcanic eruptions respectively, as calculated by the TM4-ECPL model for the present atmosphere.

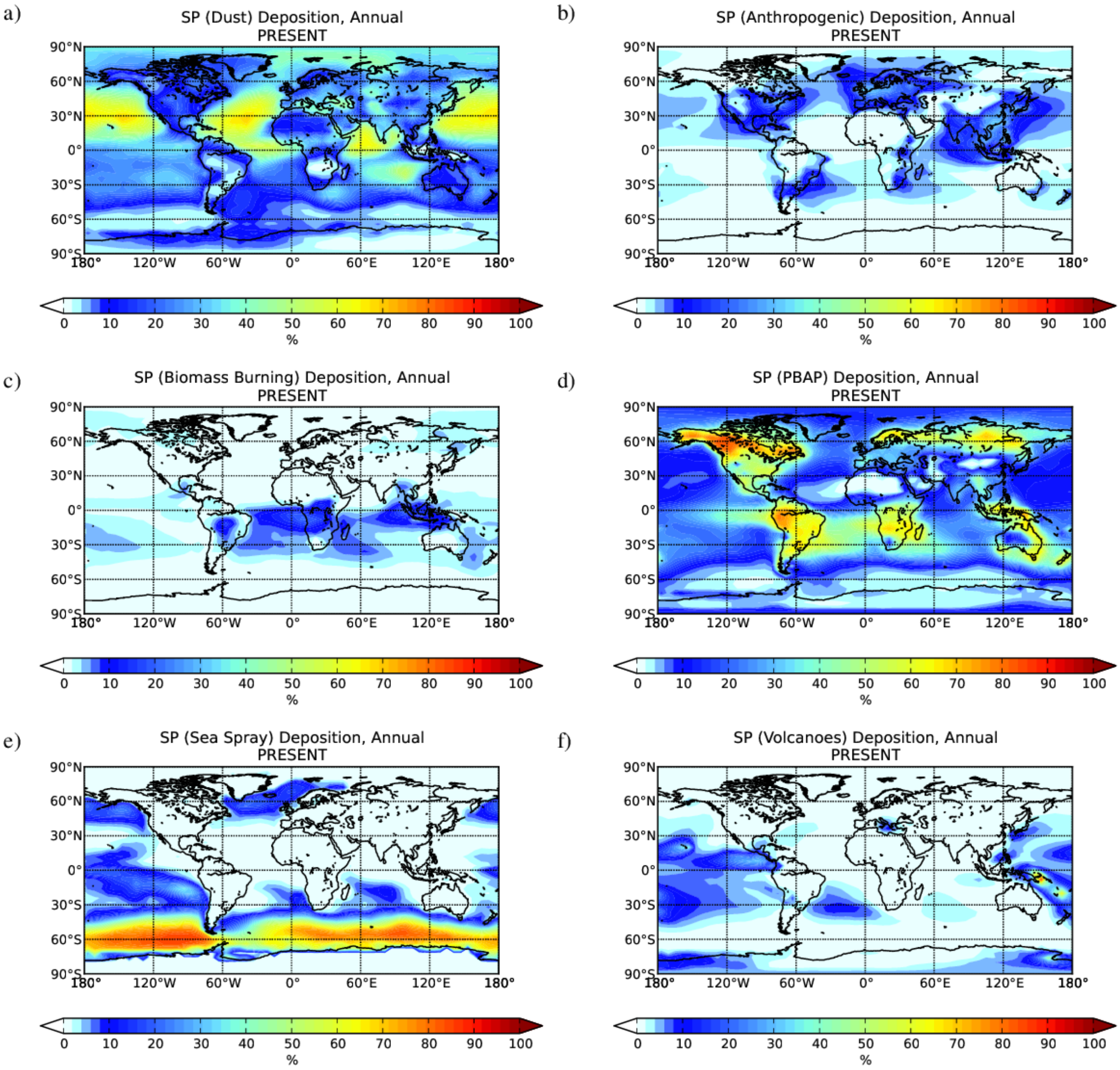

Figure S10. Calculated percentage differences of DP emissions (upper panels, a,b), apatite dissolution fluxes (middle column; b.c) and OP ageing (bottom panels; b,d) for PAST (left column a,c,e) and FUTURE (right column b,d,f) simulations compared to the PRESENT simulation (c,d).